Compact fiber-pigtailed InGaAs photoconductive antenna module for terahertz-wave generation and detection

Sang-Pil Han,[1] Namje Kim,[1] Hyunsung Ko,[1] Han-Cheol Ryu,[1] Jeong-Woo Park,[1] Young-Jong Yoon,[1] Jun-Hwan Shin,[1] Dong Hun Lee,[2] Sang-Ho Park,[2] Seok-Hwan Moon,[2] Sung-Wook Choi,[3] Hyang Sook Chun,[3] and Kyung Hyun Park[1,*]

[1]*THz Photonics Creative Research Center, ETRI, Daejeon 305-700, South Korea*
[2]*Convergence Components & Materials Research Laboratory, ETRI, Daejeon 305-700, South Korea*
[3]*Food Safety Research Division, Korea Food Research Institute, Sungnam 463-746, South Korea*
[*]*khp@etri.re.kr*

Abstract: We propose a compact fiber-pigtailed InGaAs photoconductive antenna (FPP) module having an effective heat-dissipation solution as well as a module volume of less than 0.7 cc. The heat-dissipation of the FPP modules when using a heat-conductive printed circuit board (PCB) and an aluminium nitride (AlN) submount, without any cooling systems, improve by 40% and 85%, respectively, when compared with a photoconductive antenna chip on a conventional PCB. The AlN submount is superior to those previously reported as a heat-dissipation solution. Terahertz time-domain spectroscopy (THz-TDS) using the FPP module perfectly detects the absorption lines of water vapor in free space and an α-lactose sample.

©2012 Optical Society of America

OCIS codes: (300.6495) Spectroscopy, terahertz; (260.5150) Photoconductivity; (120.4290) Nondestructive testing.

References and links

1. B. Sartorius, H. Roehle, H. Künzel, J. Böttcher, M. Schlak, D. Stanze, H. Venghaus, and M. Schell, "All-fiber terahertz time-domain spectrometer operating at 1.5 microm telecom wavelengths," Opt. Express **16**(13), 9565–9570 (2008).
2. H. Roehle, R. J. B. Dietz, H. J. Hensel, J. Böttcher, H. Künzel, D. Stanze, M. Schell, and B. Sartorius, "Next generation 1.5 microm terahertz antennas: mesa-structuring of InGaAs/InAlAs photoconductive layers," Opt. Express **18**(3), 2296–2301 (2010).
3. S.-P. Han, H. Ko, N. Kim, H.-C. Ryu, C. W. Lee, Y. A. Leem, D. Lee, M. Y. Jeon, S. K. Noh, H. S. Chun, and K. H. Park, "Optical fiber-coupled InGaAs-based terahertz time-domain spectroscopy system," Opt. Lett. **36**(16), 3094–3096 (2011).
4. C. Baker, I. S. Gregory, M. J. Evans, W. R. Tribe, E. H. Linfield, and M. Missous, "All-optoelectronic terahertz system using low-temperature-grown InGaAs photomixers," Opt. Express **13**(23), 9639–9644 (2005).
5. R. Inoue, Y. Ohno, and M. Tonouchi, "Development of fiber-coupled compact terahertz time-domain spectroscopy imaging head," Jpn. J. Appl. Phys. **45**(10A), 7928–7932 (2006).
6. Y. Lee, S. Tanaka, N. Uetake, S. Fujisaki, R. Inoue, and M. Tonouchi, "Terahertz time-domain spectrometer with module heads coupled to photonic crystal fiber," Appl. Phys. B **87**(3), 405–409 (2007).
7. C. Jördens, N. Krumbholz, T. Hasek, N. Vieweg, B. Scherger, L. Bähr, M. Mikulics, and M. Koch, "Fibre-coupled terahertz transceiver head," Electron. Lett. **44**(25), 1473–1474 (2008).
8. D. Zimdars, J. V. Rudd, and M. Warmuth, "A Compact, Fiber-Pigtailed, Terahertz Time Domain Spectroscopy System," Proc. ISSTT, 414–423 (2000).
9. J. V. Rudd and D. M. Mittleman, "Influence of substrate-lens design in terahertz time-domain spectroscopy," J. Opt. Soc. Am. B **19**(2), 319–328 (2002).
10. Y. B. Ji, E. S. Lee, S.-H. Kim, J.-H. Son, and T.-I. Jeon, "A miniaturized fiber-coupled terahertz endoscope system," Opt. Express **17**(19), 17082–17087 (2009).
11. D. Stanze, A. Deninger, A. Roggenbuck, S. Schindler, M. Schlak, and B. Sartorius, "Compact cw Terahertz Spectrometer Pumped at 1.5 μm Wavelength," J. Infrared Milli. Terahz. Waves **32**, 225–232 (2010).
12. N. Kim, J. Shin, E. Sim, C. W. Lee, D.-S. Yee, M. Y. Jeon, Y. Jang, and K. H. Park, "Monolithic dual-mode distributed feedback semiconductor laser for tunable continuous-wave terahertz generation," Opt. Express **17**(16), 13851–13859 (2009).

#168118 - $15.00 USD Received 9 May 2012; revised 6 Jul 2012; accepted 21 Jul 2012; published 27 Jul 2012

13. N. Kim, Y. A. Leem, M. Y. Jeon, C. W. Lee, S.-P. Han, D. Lee, and K. H. Park, "Widely Tunable 1.55 μm Detuned Dual Mode Laser diode for Compact Continuous-Wave THz Emitter," ETRI J. **33**(5), 810–813 (2011).
14. N. Kim, S.-P. Han, H. Ko, Y. A. Leem, H.-C. Ryu, C. W. Lee, D. Lee, M. Y. Jeon, S. K. Noh, and K. H. Park, "Tunable continuous-wave terahertz generation/detection with compact 1.55 μm detuned dual-mode laser diode and InGaAs based photomixer," Opt. Express **19**(16), 15397–15403 (2011).
15. K. H. Park, N. Kim, H. Ko, H.-C. Ryu, J.-W. Park, S.-P. Han, and M. Y. Jeon, "Portable terahertz spectrometer with InP related semiconductor photonic devices," Proc. SPIE Photonics West, Jan. (2012).
16. M. Y. Jeon, N. Kim, J. Shin, J. S. Jeong, S.-P. Han, C. W. Lee, Y. A. Leem, D.-S. Yee, H. S. Chun, and K. H. Park, "Widely tunable dual-wavelength $Er3^+$-doped fiber laser for tunable continuous-wave terahertz radiation," Opt. Express **18**(12), 12291–12297 (2010).
17. E. R. Brown, "THz generation by photomixing in ultrafast photoconductors," Int. J. High Speed Electron. Syst. **13**(02), 497–545 (2003).
18. N. S. Daghestani, S. Persheyev, M. A. Cataluna, G. Ross, and M. J. Rose, "THz generation from a nanocrystalline silicon-based photoconductive device," Semicond. Sci. Technol. **26**(7), 075015 (2011).
19. A. Danylov, "THz laboratory measurements of atmospheric absorption between 6% and 52% relative humidity," Submillimeter-Wave Technology Laboratory University of Massachusetts Lowell, 175 Cabot Street, Suite 130, Lowell, MA 01854, http://stl.uml.edu, Sep. (2006).
20. A. Roggenbuck, H. Schmitz, A. Deninger, I. Cámara Mayorga, J. Hemberger, R. Güsten, and M. Grüninger, "Coherent broadband continuous-wave terahertz spectroscopy on solid-state samples," New J. Phys. **12**(4), 043017 (2010).
21. E. R. Brown, J. E. Bjarnason, A. M. Fedor, and T. M. Korter, "On the strong and narrow absorption signature in lactose at 0.53THz," Appl. Phys. Lett. **90**(6), 061908 (2007).

1. Introduction

Compact, lightweight, and cost-effective terahertz (THz) spectroscopy and imaging systems have gradually become desired for use in outdoors or mobile situations such as in the fields of security, non-invasive testing, food and agricultural goods quality control, and environmental monitoring. Fiber-coupled THz systems are one of the solutions. They have lower cost, higher stability, and more portable compared with free-space THz systems, because they have movable THz emitters and detectors [1].

Recently, a number of compact THz emitting and detecting systems and their component modules have been developed. In such systems, there have been various descriptions of fiber-coupled THz spectrometers [1–7]. Owing to the versatility of their long-wavelength optical components, compact size, and cost-effectiveness, InGaAs-based fiber-coupled terahertz time-domain spectroscopy (THz-TDS) systems such as those presented in refs [1–3]. are considered promising. Three types of fiber-connected photoconductive antenna (PCA) modules for these systems have been introduced [8–11]. One is a butterfly-type fiber-pigtailed THz transmitter module measuring 1" × 0.5" × 0.5" and weighing a couple of ounces [8,9]. Another comprises miniaturized THz generator and detector heads whose electrical and optical parts are fixed by epoxy in the limited volume of the module [10]. The third has two input optical fibers connected to the THz emitter and receiver, respectively, but they can be adjusted using built-in adjustment screws [11]. In addition, compact and broadband continuous-wave (CW) THz optical beat sources such as a monolithic dual-mode distributed feedback semiconductor laser, 1.55 μm detuned dual-mode laser diode, and dual-wavelength Er^{3+}-doped fiber laser have been also developed to realize handheld THz modules [12–16].

In this paper, we propose a compact fiber-pigtailed InGaAs PCA (FPP) module having a small form factor and a highly heat-conductive submount. Temperature distribution images of the fabricated PCA chips were observed by a mid-infrared (MIR) camera. Finally, we present the experimental results of THz-TDS measurements of free space water vapor and of an α-lactose sample, using the proposed FPP module.

2. Fiber-pigtailed InGaAs PCA module

Figures 1(a) and 1(b) show a photograph of this FPP module and its cross-sectional schematic view, respectively. The FPP module consists of a log–spiral antenna-integrated low-temperature grown (LTG) InGaAs PCA chip, heat-conductive submount, high-resistivity hyper-hemispherical Si lens, single-mode fiber assembly with an aspherical glass lens (A-

#168118 - $15.00 USD Received 9 May 2012; revised 6 Jul 2012; accepted 21 Jul 2012; published 27 Jul 2012
(C) 2012 OSA

lens), a miniature coaxial cable, and a module housing. The assembly process of the FPP module was as follows: First, the PCA chip and the heat-conductive submount were bonded together using a flip-chip bonding process. Then, the submount was attached onto the body of the module housing, and the bias pads of the submount were connected with a miniature coaxial cable. A Si lens was placed on the bottom surface of the PCA chip, and fixed with the cover screw of the module housing. Finally, the entire module housing was actively aligned and welded to the fiber assembly with the A-lens, using a laser welding technique. We note that the active-alignment between the active area of the PCA chip and the fiber core of the fiber assembly must be precise before laser welding. The active-alignment was necessary to monitor and find the maximum value of the PCA photocurrent, when a bias voltage of 0.1 V was applied and an optical beam with a power of 5 dBm was adjusted and focused to the active area of the PCA chip.

The proposed FPP module has a small form factor, with a volume as small as under 0.7 cc, which does not include the single-mode fiber assembled with ferrule and boot. The heat-conductive submount in the module adopts a specially designed heat dissipation structure for cooling the active area of the PCA chip. It needs to effectively dissipate heat generated at the active area of the PCA during operation, because generated heat can be one factor that degrades the performance of the InGaAs PCA. As depicted in Fig. 1(b), the A-lens in the fiber assembly was tilted at an angle of 4° toward the PCA chip to reduce the return loss to less than −40 dB.

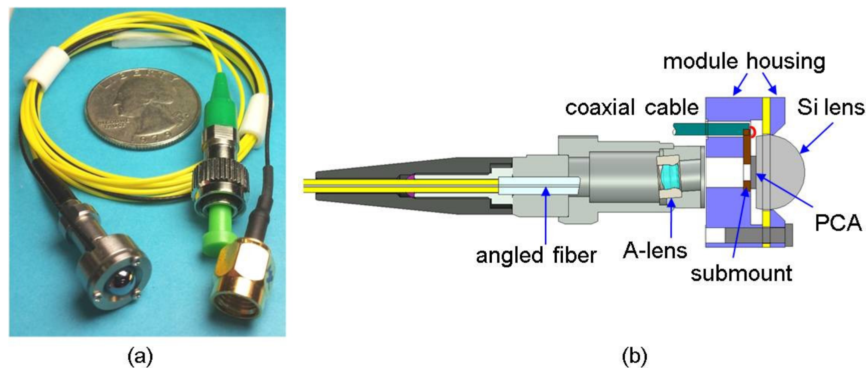

Fig. 1. (a) Photograph of fiber-pigtailed InGaAs PCA (FPP) module and (b) cross-sectional schematic view of FPP module.

The LTG-InGaAs PCA assembled in the FPP module was fabricated through the following process: A 1.2-μm-thick Be-doped InGaAs layer was low-temperature grown on semi-insulating InP substrates using a molecular beam epitaxy (MBE) system. The surface of the LTG-InGaAs layer was passivated using a SiN_x layer to reduce dark current, except for a central active area of about 10×10 μm^2. An antenna and 10 solder pads were then formed by depositing 30-nm-thick Ti, 10-nm-thick Pt, and 450-nm-thick Au. The 10 solder pads were used to bond the PCA chip onto the submount using the flip-chip bonding process. To increase the electric field strength at the active area, an interdigitated finger structure can additionally be formed. A 200-nm-thick SiN_x layer was deposited as an anti-reflection coating and solder dams. The SiN_x layer deposited on the solder pads of 10 circles, as shown in Fig. 2, was patterned and removed to form the solder dams, which were used to suppress the spreading-out of solders when they reflow during heating. The carrier lifetime of the LTG-InGaAs PCA sample was measured to be 1.7 ps. The size and thickness of the LTG-InGaAs PCA were 2.2×2.2 mm^2 and 0.35 mm, respectively. The fabricated LTG-InGaAs PCA and the schematic of the solder dams are in Fig. 2.

#168118 - $15.00 USD Received 9 May 2012; revised 6 Jul 2012; accepted 21 Jul 2012; published 27 Jul 2012
(C) 2012 OSA

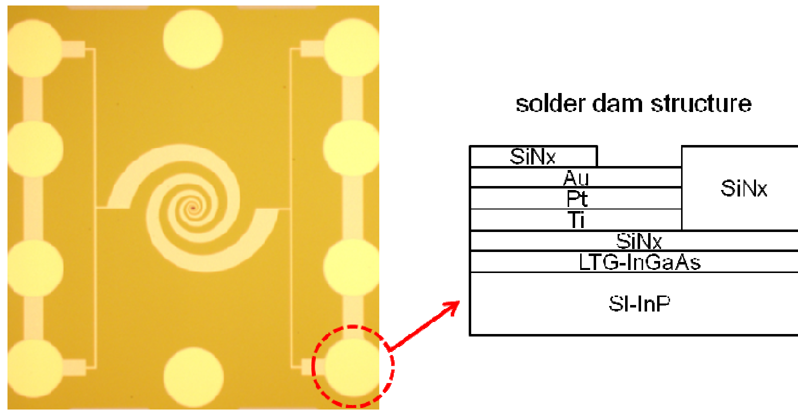

Fig. 2. Microscopic image of LTG-InGaAs PCA and schematic of solder dam

We used two types of heat-conductive submounts. The first was a heat-conductive printed circuit board (PCB) submount, the diameter and thickness of which were 7 mm and 1 mm, respectively. Heat transfers through a plurality of grounds (GND) via-holes and GND planes connected to the solder pads of the PCB. The GND plane of the bottom side of the PCB was attached onto the body of the module-housing using a thin coating of silver epoxy. Using the flip-chip bonding process depicted in Fig. 3(a), the PCA chip and the PCB were connected electrically and mechanically. The solder pads of the PCA chip and the solder balls of the PCB were bonded in self-passive alignment at a defined temperature and time (for example, 240 °C, 25 s). Shear strength test results, shown in Fig. 3(b), were observed to be as good as around 3 kgf (MIL-STD-833 compliance: 2.5 kgf) when the number of PCB solder balls used was 10. It was clear that to satisfy the MIL spec., the number of solder balls should be equal to or greater than 10.

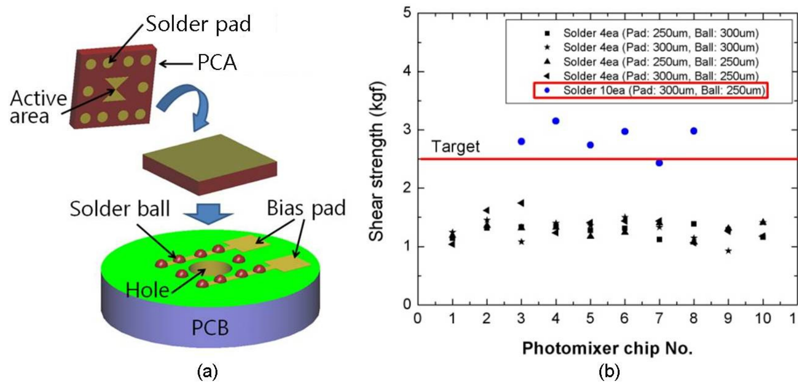

Fig. 3. (a) Flip-chip bonding process and (b) shear strength test results for various solder and pad sizes and number of solder balls of PCB.

The second type of submount was an aluminium nitride (AlN) submount. We chose the number of solders as 10 based on the above shear strength test results of the heat-conductive PCB. The dimensions and thickness of the AlN submount were 4 × 3 mm^2 and 0.5 mm, respectively. The central hole and the half-circle outer hole in the AlN submount were used for optical coupling and electrical cabling, respectively, and were formed by laser drilling. AuSn (5-µm-thick) as the solder and TiW/Pd/Au as the solder pad base metal were patterned and deposited on the AlN submount surface. Figures 4(a) and 4(b) show photographs of an AlN submount before and after bonding to a PCA chip by the flip-chip bonding process

#168118 - $15.00 USD Received 9 May 2012; revised 6 Jul 2012; accepted 21 Jul 2012; published 27 Jul 2012
(C) 2012 OSA

(Kalsuss, FC150) using a heating temperature of 320 °C and a heating time of 60 s. The shear strength of the AlN submount was considerably higher than that of the heat-conductive PCB.

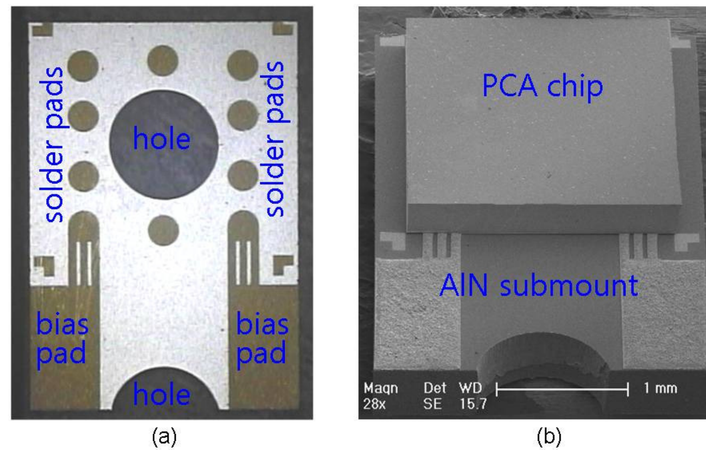

Fig. 4. (a) Photograph of fabricated AlN submount and (b) SEM image after bonding to PCA chip by flip-chip bonding process, where heating temperature and heating time were 320 °C and 60 sec, respectively.

3. Thermal characteristics of the FPP module

Heat generated in the active area of the PCA must be dissipated to increase SNR and performance in THz systems; inefficient heat dissipation from the PCA will result in thermal degradation. Thermal degradation is one of the factors that limit PCA performance. The sources of this heat are the optical energy absorbed by the active area of the PCA and joule heating due to the photocurrent. Furthermore, in narrow-band-gap materials such as InGaAs, the THz output power of the PCA can also be limited by joule heating from the dark current [17]. Therefore, heat dissipation is vital for InGaAs PCAs because the bias voltage applied at the PCA is limited by the heat generated due to the electrical current [18].

First, we obtained temperature distribution images using a MIR camera (FLIR Systems, Thermo Vision A40M) for three different PCA chip configurations to investigate their dynamic heat characteristics. These three configurations were a PCA chip only, a PCA chip on the heat-conductive PCB, and a PCA chip on the AlN submount, operated under the same conditions with an optical CW pumping power of 19 dBm and a bias of 3 V. The compliance current was 2 mA. The temperature distribution images are shown in Fig. 5. In the case of the PCA chip only, which was laid on a PCB substrate without any heat-conductive submounts, the surface temperature of the chip increased by up to 7 °C. In the case of the PCA chip on the heat-conductive PCB, the surface temperature of the chip increased by 3 °C. For PCA chip on the AlN submount, the surface temperature of the chip increased by less than 1 °C. As a result, the amounts of heat-dissipation of the FPP modules due to using the heat-conductive PCB and the AlN submount without any cooling systems improved by 40% and 85%, respectively, when compared to the PCA chip only. Furthermore, the measured current of the PCA chip on the AlN submount increased only by a negligible amount. However, both currents for the PCA chip only and the PCA chip on the heat-conductive PCB continuously increased until the compliance current was reached. These results confirmed that not only the AlN submount would be an excellent heat dissipation solution but that the heat-conductive PCB would also be good.

#168118 - $15.00 USD Received 9 May 2012; revised 6 Jul 2012; accepted 21 Jul 2012; published 27 Jul 2012
(C) 2012 OSA

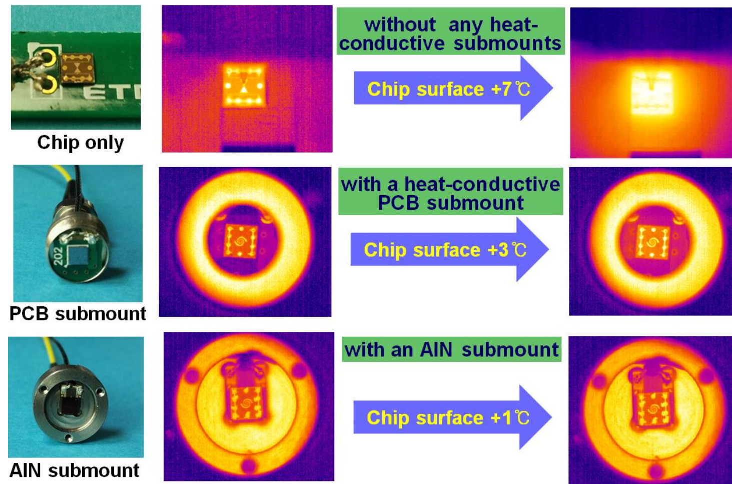

Fig. 5. Temperature distribution images for three PCA chip configurations, taken with a MIR camera when optical pumping power of 19 dBm and bias of 3 V were applied to the chips. The compliance current was limited to 2 mA.

We also measured THz signal as a function of photocurrent for two FPP emitter modules with different submounts to verify which submount was more effective, using our THz-TDS setup [3]. The emitter photocurrent was controlled by a certain amount of bias voltage which was maintained for 10 min every step. In the case of the heat-conductive PCB submount, when emitter photocurrent reached about 5.9 mA, it abruptly increased up to a compliance current of 10 mA and THz signal simultaneously decreased from 1.76 nA to 1.62 nA, as shown in Fig. 6. However, there was no a dramatic increase point of emitter photocurrent until a compliance current of 10 mA for the AlN submount.

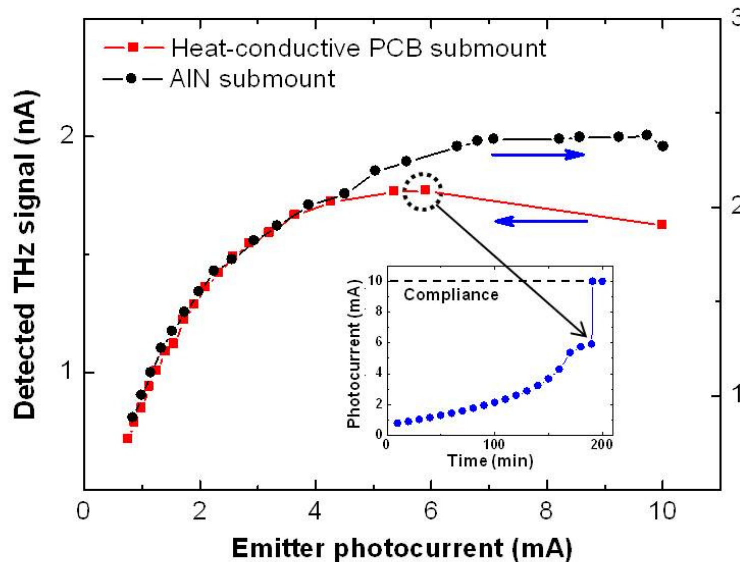

Fig. 6. Detected THz signal as a function of photocurrent for two FPP emitter modules with different submounts, with inset showing emitter photocurrent characteristics for the heat-conductive PCB submount, where a certain amount of bias voltage increases every 10 min.

#168118 - $15.00 USD Received 9 May 2012; revised 6 Jul 2012; accepted 21 Jul 2012; published 27 Jul 2012
(C) 2012 OSA

4. Experimental results of THz-TDS

We set up a fiber-coupled THz-TDS system using the FPP modules with the AlN submounts as emitter and detector. Divergence-type Si lenses in the modules and two parabolic mirrors in the system were used to generate a collimated THz wave. The free-space distance between the emitter and the detector in the THz-TDS setup was 210 mm. An optical average pumping power of 9 dBm, optical average probing power of 6 dBm, a bias peak-to-peak voltage of –10–10 V, and an emitter photocurrent of 0.6 mA were applied to the THz-TDS setup.

Figure 7(a) shows time trace data of free space measured using the THz-TDS containing the FPP module, and Fig. 7(b) is its corresponding fast Fourier transform (FFT) amplitude spectrum, where the time delay step and the frequency resolution were 0.1 ps and 2.44 GHz, respectively. The multi-poled time signal trace observed in Fig. 7(a) is estimated to be due to the log-spiral antenna. As shown in Fig. 7(b), absorption lines of water vapor in the free space were clearly detected at 557, 752, 988, 1097, 1113, 1163, 1208, 1229, 1411, 1602, 1661, 1669, 1717, and 1762 GHz in conditions of a relative humidity of about 40% and room temperature [19]. These results show that the THz radiation bandwidth of the fabricated FPP modules will likely be sufficiently higher than 2 THz.

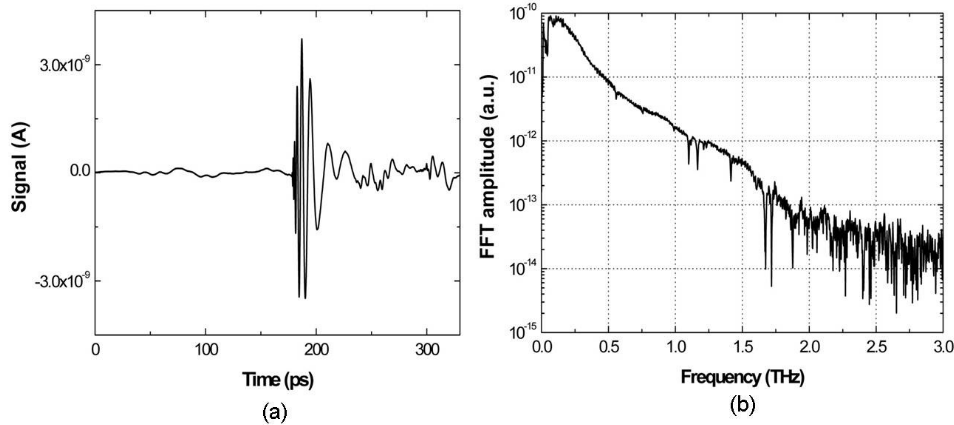

Fig. 7. (a) Time trace data of free space and (b) its FFT amplitude spectrum measured using fiber-coupled THz-TDS containing FPP module. The time delay step and the frequency resolution were 0.1 ps and 2.44 GHz, respectively.

We prepared α-lactose and polyethylene (PE) pellets as test and reference samples, respectively. Figure 8(a) shows the FFT amplitude spectra of a 100% PE sample and a 10% α-lactose sample containing a 90% PE (the identical weight of the above 100% PE) with thicknesses of 3.19 and 3.35 mm, respectively. The test and reference samples were placed and measured at the center position between the two parabolic mirrors. Figure 8(b) shows the absorption coefficient of the α-lactose sample as calculated from the results in Fig. 8(a). As shown in Fig. 8(b), absorption lines of α-lactose were finely resolved at 532, 1198, and 1369 GHz [20,21].

#168118 - $15.00 USD Received 9 May 2012; revised 6 Jul 2012; accepted 21 Jul 2012; published 27 Jul 2012
(C) 2012 OSA

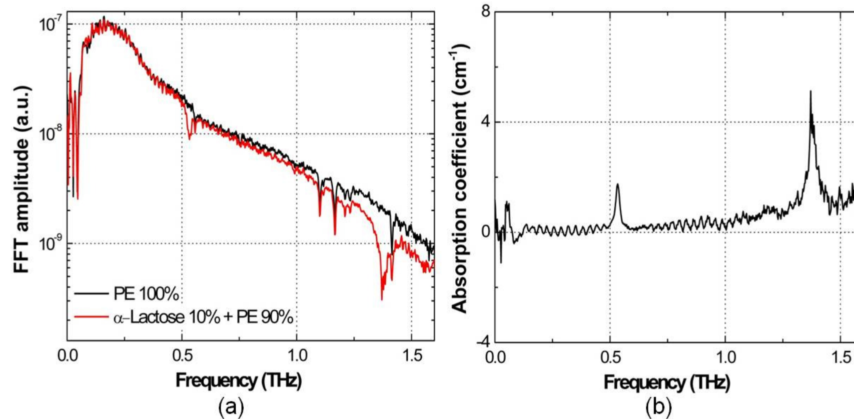

Fig. 8. (a) FFT amplitude spectra and (b) absorption coefficient of α-lactose sample, obtained from fiber-coupled THz-TDS containing FPP module. The time delay step and the frequency resolution were 0.1 ps and 2.44 GHz, respectively.

5. Summary

We have proposed a compact fiber-pigtailed InGaAs PCA (FFP) module. The module has a small volume of less than 0.7 cc, integrated and connected to single-mode fiber for optical input and a miniature coaxial cable for electrical input. The FFP module also has an effective heat dissipation solution. According to experimental results, the amounts of heat-dissipation of the FPP module due to use of either a heat-conductive PCB or an AlN submount, without any cooling systems, were improved by 40% and 85%, respectively, when compared with a PCA chip on a conventional PCB. The THz-TDS using the FPP module with the AlN submount finely detected absorption lines of nearly 2 THz for water vapor in free space, and 532, 1198, and 1369 GHz for an α-lactose sample. These results showed that the capability of the fabricated FFP module would likely be sufficiently greater than 2 THz.

Acknowledgments

This work was supported by the Joint Research Projects of ISTK and the Public welfare & Safety research program through National Research Foundation of Korea (NRF), by the Ministry of Education, Science and Technology- grant #2010-0020822.

#168118 - $15.00 USD Received 9 May 2012; revised 6 Jul 2012; accepted 21 Jul 2012; published 27 Jul 2012
(C) 2012 OSA